Online Appendix

A Additional Empirical Results

A.1 SafeGraph Data

We complement this analysis with data from SafeGraph.[18] Among other things, SafeGraph provides disaggregated and detailed high-frequency information on individual travel in the US. The underlying data source is a panel of opt-in, anonymized smartphone devices, and is well balanced across US demographics and space.

In early April 2020, SafeGraph made several datasets freely available to researchers.[19] The main dataset we use is their first "COVID-19 Response Dataset," named "Weekly Patterns (v2)." This registers GPS-identified visits to Points of Interest (POIs) (primarily businesses) with an exact known location in the US at an hourly frequency in a balanced panel. We use data covering the time period from March 1 to September 27, 2020. The dataset is large: on March 1, the dataset recorded approximately 32.1 million individual visits to approximately 3.9 million POIs.

For each state and the District of Columbia, we count the total number of visits to POIs during each day. We express this variable as a percent change from a baseline week, the corresponding day during the first week of March. This gives us, for each state, a measure of the decline of social activity that naturally maps to the model. Figure 8 reports our results. We again plot thin lines for each state, as well as a thicker line for the median across states. The figure shows a remarkably uniform contraction of social activity across US states beginning on March 13 and leveling off fifty percent below the baseline towards the end of March.

One might be concerned that the decline in social activity reflects the closure of POIs rather than self-imposed restrictions on activity. To address this, we use SafeGraph data to construct a measure of POI closures in March 2020 and then show that foot traffic declined substantially prior to closure; see appendix A.4.

[18] Attribution: SafeGraph, a data company that aggregates anonymized location data from numerous applications in order to provide insights about physical places. To enhance privacy, SafeGraph excludes census block group information if fewer than five devices visited an establishment in a month from a given census block group.

[19] For detailed information on the datasets we use, see `https://docs.safegraph.com/docs/weekly-patterns` and `https://docs.safegraph.com/docs/social-distancing-metrics`.

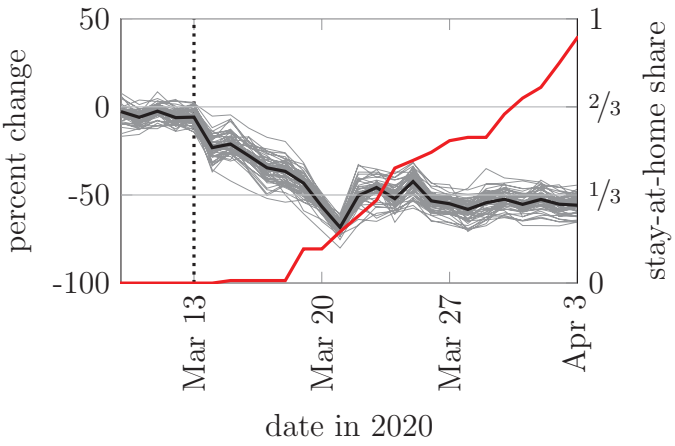

Notes: Visits to Points of Interest in SafeGraph's "Weekly Patterns" COVID-19 Response Dataset. We sum daily visits within each state and report the percent decline from the same day during the baseline week (first week of March 2020). Each thin line corresponds to one of the 51 US states and the District of Columbia. The thick black line marks the median state in terms of the decline relative to baseline at any given day. The solid red line is the percent of the population subject to stay-at-home or shelter-in-place orders, indicated on the right-hand axis. The population subject to these orders is based on authors' own calculations using `https://www.nytimes.com/interactive/2020/us/coronavirus-stay-at-home-order.html`. The vertical dotted line indicates March 13, 2020, the date of the declaration of national emergency.

Figure 8: Declining Activity, Early and Everywhere III

A.2 Social Activity — Crunch, Recovery, and Second Wave

Figure 9 shows the full data range for the SafeGraph data. Like in the Google data, we see a sluggish recovery throughout the spring and summer that remains incomplete in the fall.

Figure 10 shows the same across the Copenhagen, Oslo, Stockholm, and Chicago in the Google data (which run until February 13, 2021). It is worth noting that Stockholm, after a milder initial crunch experiences a more sustained depression of activity throughout the summer, consistent with a higher stock of infections. Like for the 50 US states depicted in the main text, we see a substantial second wave of social distancing in the fall and winter of 2020–21.

Finally, we note that in recent work that succeeded ours, Goolsbee and Syverson (2020) use SafeGraph data and conclude that, while social activity fell by 60 percentage points, stay-at-home orders explain only 7 percentage points of that.

A.3 Additional Mobility Metrics — Time at Home

SafeGraph has a second data set named "Social Distancing Metrics." It assigns smartphones a home address using their night-time location and then considers individual foot traffic. We use data covering the time period from March 2, 2020 to September 28, 2020. Again, the

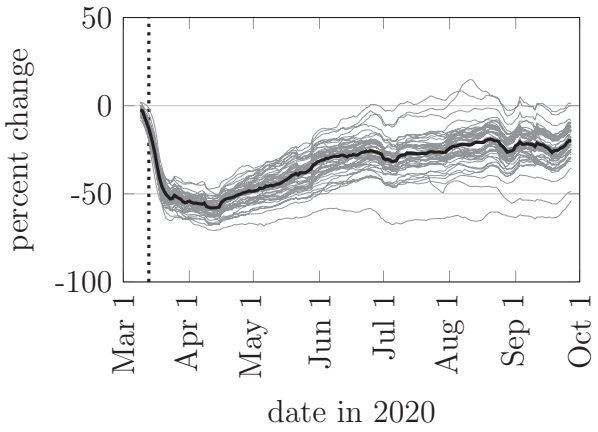

Notes: Identical to Figure 8, but for a wider date range and a 7 day centered moving average.

Figure 9: Crunch and Recovery

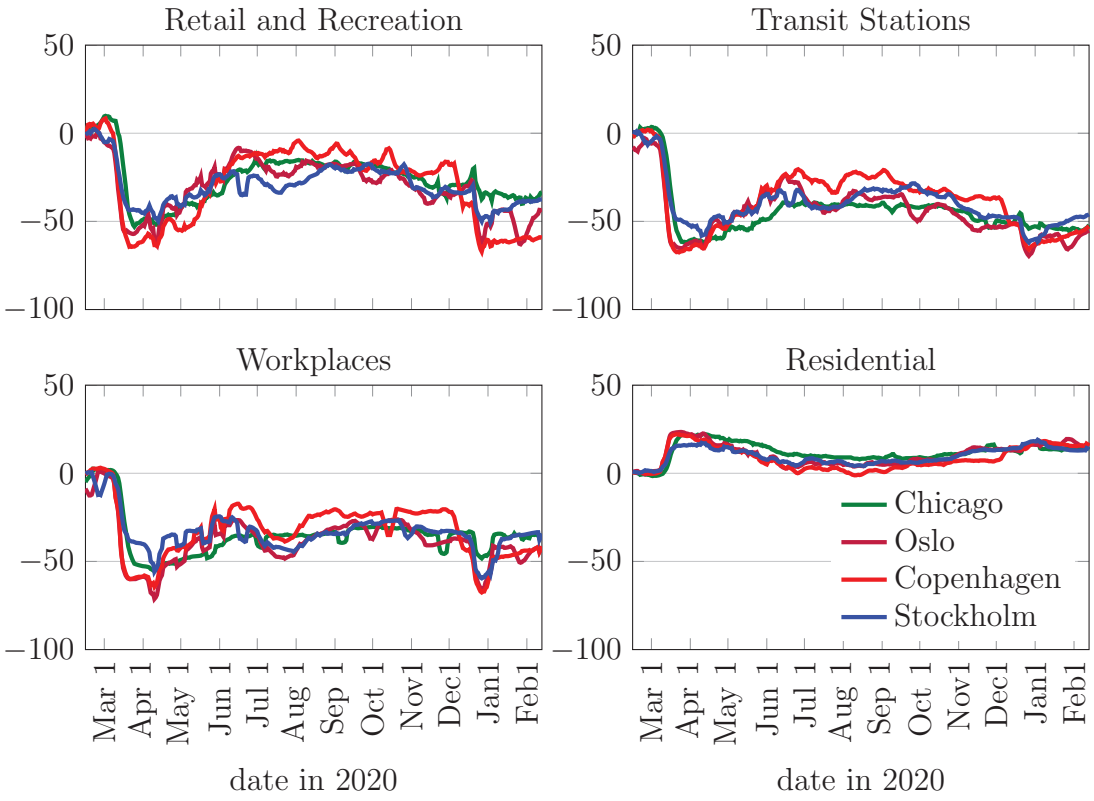

Notes: Figure identical to Figure 2 but with a wider date range and a 7 day centered moving average.

Figure 10: Crunch and Recovery across Space — Google Data

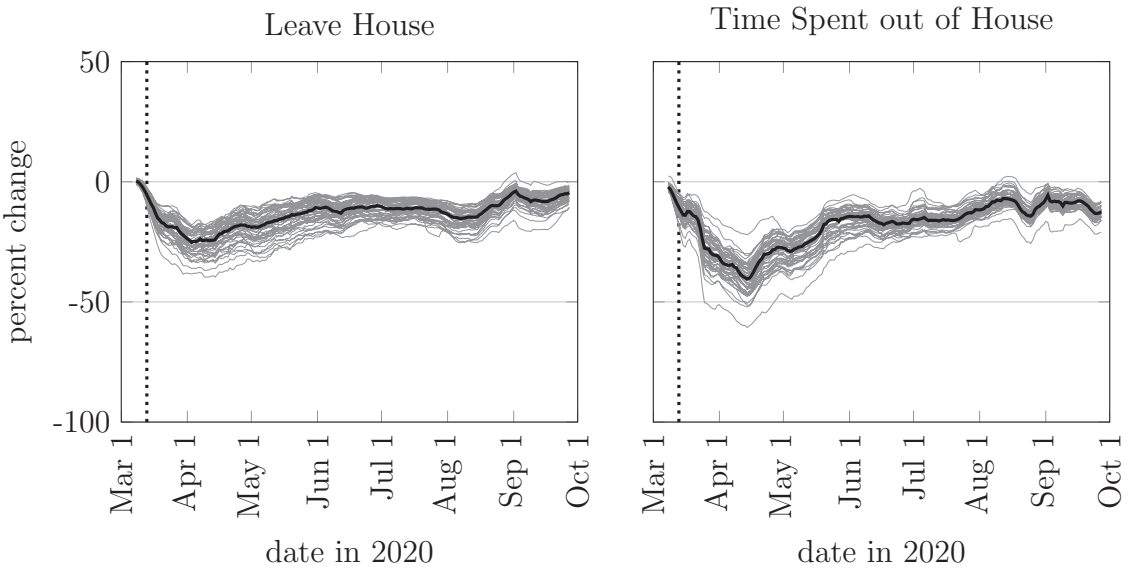

Notes: Social activity based on SafeGraph's "Social Distancing Metrics" COVID-19 Response Dataset. Left Panel Metric: Fraction of devices that leave assigned "home" at least once during any day. Right Panel Metric: One minus fraction of time spent at home location of median device. Metrics computed at census block level, then averaged to the state level (with device-count as weight). Each thin line corresponds to one of the 51 US states and the District of Columbia. The thick black line marks the median state in terms of the decline relative to baseline at any given day. Each correspond to 7 day centered moving averages. The vertical dotted line indicates March 13, 2020, the date of the declaration of national emergency.

Figure 11: Social Activity, Additional Metrics

data set is large. On March 2, the dataset contains information from over 20 million devices across 220,000 census block groups with at least 5 devices. Among other things, it reports, for each census block group, the median number of minutes a device dwells at its home location (variable median_home_dwell_time). In addition, it also measures the number of devices that spend the entire day at the home location (variable completely_home_device_count).

We proceed in the same fashion as with our main measure. We subtract the median minutes spent at home from $24 \times 60 = 1440$ and take a daily state-wide average across census block groups using the device count as weights. We similarly construct the state-wide fraction of all devices that leave the house at least once during any day. Both are expressed relative to a benchmark of the first week of March. Figure 11 plots the evolution of these two metrics the same way as Figure 8 does for our main variable.

A.4 Closures

We only work with data covering the first four weeks of March 2020 since this part of the exercise focuses on the sharp initial decline in social activity in that period. We work with

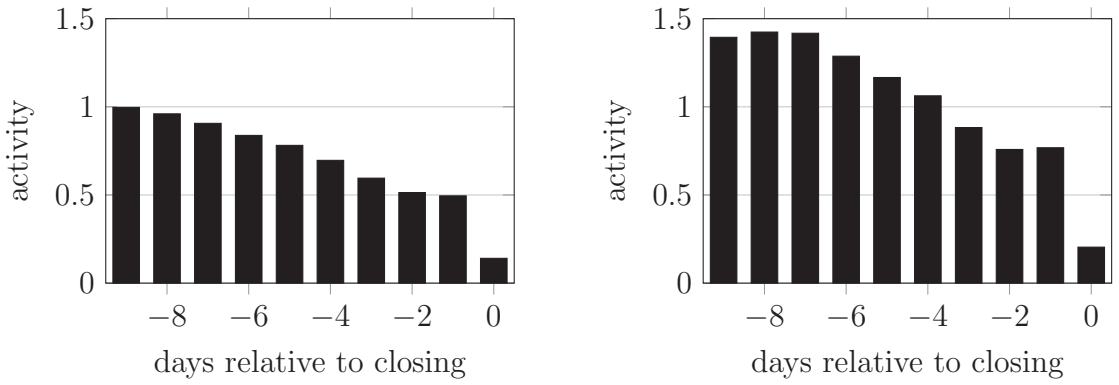

Notes: NAICS codes 44, 45, 71, 72 only. Activity data covering the first four weeks of March 2020 only. Only POIs with at least 10 average daily visitors during first week of March and only POIs which are covered all days. POI closure identified on first of first three consecutive days where daily traffic is below 20 percent of average daily traffic during baseline week (first week of March 2020). Closures March 11 and after. The left panel plots the number of daily visits relative to same day-of-week during baseline period (first week of March). The right panel does the same but only for POIs that, in the baseline week, receive at least 50 percent of their total traffic on the weekend.

Figure 12: Declining POI Visits Prior to Closing Date

the following closure criterion. We diagnose a POI as closed on the first of three consecutive days where daily traffic never exceeds 20 percent of the average daily traffic during a baseline period (first week of March). We only use POIs with 10 or more average daily visitors during baseline which are covered during all days the dataset covers and restrict attention to NAICS codes 44, 45, 71, 72 (retail trade; arts, entertainment, and recreation; accommodation and food services). Proceeding this way, we find that 20.6% of the 1,012,502 POIs had closed by the end of the sample.

In Figure 12 (left panel) we plot the average daily traffic (relative to same day-of-week traffic during baseline) in the 10 days prior to store closure. The main takeaway is that, prior to store closure revealed in this fashion, foot traffic to POIs declined substantially. This suggests that closures are not the driving force of the decline in activity that preceded the official lockdown measures.

One concern is that the pre-closure decline may reflect the closure of other businesses or offices. To address this, we separately restrict attention to POIs that receive, in the baseline week, over 50 percent of their traffic on Saturdays and Sundays. We plot the corresponding decline in pre-closure traffic in the right panel. The basic picture remains the same, although notably visits to "weekend places" were higher than normal until a few days before they shut down.

B Computational Algorithm

We seek to solve the model with $\alpha \in [0,1]$, as described in 4.4. Recall that $\alpha = 0$ corresponds to the laissez-faire equilibrium and $\alpha = 1$ corresponds to the planner's problem. The model is described by the state equations (7)–(8), the optimality condition (18), the costate equations (19)–(20), and the transversality condition (21).

Note that if $u(a) = \log a - a + 1$ or $u(a) = -(1-a)^2/2$, we can solve equation (18) explicitly for $A(t)$ as a function of the state and costate variables. We use this in our solution and so have a system of four ordinary differential equations.

Our main computational approach numerically solves the state and costate equations using a backward shooting algorithm. We normalize the terminal date to 0 and set $N_i(0) = 10^{-9}$. We then pin down the terminal values of the costate variables by solving equations (19)–(20) with $A(0) = 1$ and $\lambda_s'(0) = \lambda_i'(0) = 0$. Imposing that the co-state are stationary at the terminal date ensures that we are not picking an explosive path and so the transversality condition is (approximately) satisfied Note that the solution to the differential equation system is not very sensitive to the terminal values of the costate variables, particularly at dates in the distant past. This is natural since the initial evolution of the pandemic under individual optimal behavior and planner should not be sensitive to the shadow cost of infection in the far away future. It is also reassuring since, of course, $A(0) = 1$ and $\lambda_s'(0) = \lambda_i'(0) = 0$ do not *exactly* hold at the finite terminal date.

Finally, we search for the terminal value $N_s(0)$. For a given value of $N_s(0)$, we can numerically solve the differential equation system backwards through time. Our aim is to solve backwards to an unknown time $T < 0$ with a known value of $N_s(T)$ and $N_i(T)$, e.g. $N_s(T) = 0.9999223$ and $N_i(T) = 0.0000527$ in our benchmark calibration. If our guess of $N_s(0)$ is too large, we find that there is a finite date t with $N_s(t) = 0.9999223$ and $N_i(t) > 0.0000527$. If our guess of $N_s(0)$ is too small, we find that there is a finite date t with $N_s(t) < 0.9999223$ and $N_i(t) = 0.0000527$. Thus we can easily search for the value of $N_s(0)$ that takes us back to the desired initial condition.

A difficulty arises because the state equations are unstable when we solve backwards in time. Given issues of numerical precision, this means that we may not be able to find a value of $N_s(0)$ for which $N_s(T) = 0.9999223$ and $N_i(T) = 0.0000527$. Instead, two nearby values may lead to widely divergent paths. We illustrate this with the blue lines in Figure 13. The two paths are similar for a while, but ultimately diverge by a substantial amount. The correct value of $N_s(0)$ lies in between the value on these two curves, but we are unable to find it directly.

Instead, we look for the first time that the two paths diverge substantially, defined as

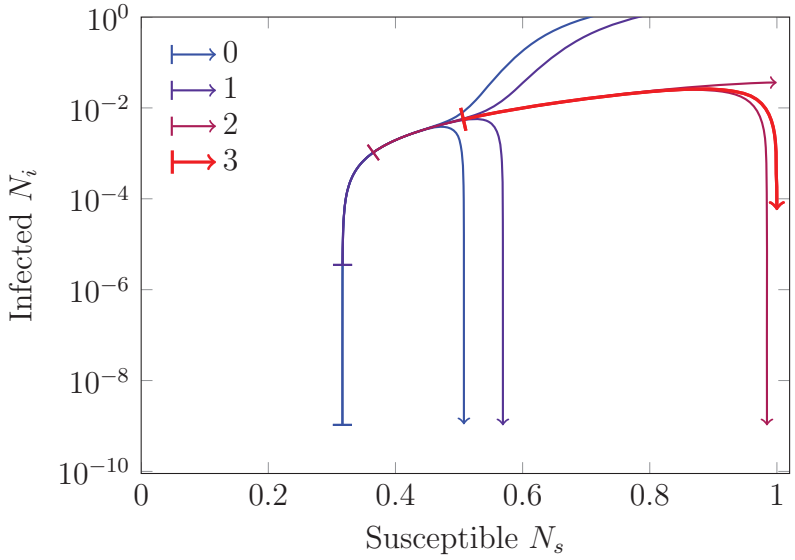

Notes: The figure corresponds to the laissez-faire version of the model ($\alpha = 0$) in the baseline calibration.

Figure 13: Saddle Path

the ratio of any of N_s, N_i, λ_s, and λ_i across the two paths exceeding a tolerance threshold, which we set to 10^{-6}. Call the first (i.e. least negative) date when this occurs T_1. We have now found the solution to the differential equation between T_1 and 0. We then fix the value of N_i, λ_s, and λ_i at the saddle path value at T_1 and again search for the value of $N_s(T_1)$ which takes us back to our desired initial condition, e.g. $N_s(T) = 0.9999223$ and $N_i(T) = 0.0000527$. Once again, we may find two paths near the saddle path which diverge by an amount that exceeds our tolerance. In this case, we call the first (least negative) such date T_2 and repeat the procedure.

Figure 13 plots the joint path of the state variables under laissez-faire and our main calibration. We highlight three of the splits.[20] The path labeled '1' starts at $T_1 = -3050$ with $N_s(T_1) = 0.317$ and $N_i(T_1) = 0.00000332$. The path labeled '2' starts at $T_2 = -5110$ with $N_s(T_2) = 0.364$ and $N_i(T_2) = 0.00101$. Finally, the red path label '3' starts at $T_3 = -5520$ with $N_s(T_3) = 0.504$ and $N_i(T_3) = 0.00551$. This one reaches $N_s(T) = 0.9999223$ and $N_i(T) = 0.0000527$ at $T = -5786$, our desired terminal condition.

Finally, in plotting the results in the text, we use an alternative normalization of time, defining date T to be March 13, 2020. This does not require resolving the model, just changing the time index.

[20] In fact, there are five splits in total. The first two splits occur very early on, and we do not plot them.

	Laissez-Faire			Optimum		
Calibration	Health	Activity	Total	Health	Activity	Total
Baseline	\$11,374	\$1,277	\$12,652	\$860	\$7,227	\$8,087
$u(a) = -\frac{1}{2}(1-a)^2$	\$9,948	\$1,435	\$11,384	\$214	\$5,616	\$5,830
$\kappa = 98.5$	\$6,763	\$611	\$7,373	\$3,942	\$2,358	\$6,300
$R_0 = 6.4$	\$15,973	\$1,799	\$17,772	\$8,776	\$6,630	\$15,406
$\delta = 0.33/365$	\$13,541	\$1,293	\$14,834	\$7,883	\$4,735	\$12,618
$N_i(0) = 0.01$	\$11,745	\$1,327	\$13,072	\$1,852	\$7,164	\$9,016

Notes: Columns 1 and 4: present value of per capita pure health cost of disease. Columns 2 and 5: present value of per capita cost of reduction in social activity. Columns 3 and 6: total cost. First three columns are for the laissez-faire equilibrium, last three are for the optimum. Each row corresponds to a different calibration. We convert utils to US dollars using a factor of 123, as discussed in Section 5.1.

Table 3: Per Capita Welfare Cost of Disease: Robustness

C Robustness

C.1 Robustness to Parameters and Functional Forms

In this section, we show the laissez-faire and optimal dynamics with reasonable changes to most of the parameters. Given the large uncertainty around many of the key model parameters, fairly large changes are reasonable. We find that our main findings are robust to alternative parameter choices. In particular, we find a strong laissez-faire equilibrium reduction in social activity; an immediate and persistent optimal reduction in social activity that only disappears in the very long run; and an optimal path that keeps the effective reproduction number very close to 1 after peak infections.

While the equilibrium amount of social distancing and the health costs of the pandemic are robust to parameter changes, we find some sensitivity under the optimal policy. Table 3 summarizes the total cost under both equilibrium and optimum, along with their breakdown into health and activity cost. When the gains from social distancing are smaller because the health cost of infection κ is lower or the arrival rate of a cure δ is lower, we find that optimal policy allows for an initial wave of infections. The same thing happens when the basic reproduction number R_0 is higher.

To understand this dichotomous feature of optimal policy, note that the pandemic always eventually gets to a place where infections are slowly rolled over, with R_t close to 1. Mechanically, when $\beta > \gamma$, setting $R_t = 1$ requires some combination of social distancing ($A < 1$) and a reduction in the number of susceptible people ($N_s < 1$). If the discounted marginal cost of social distancing, $u'(A)/(\rho + \delta)$, is too high relative to the health benefits of avoiding an infection, κ, then the planner allows for an initial wave of infections, a higher

level of A which reduces N_s. Once N_s is down to a level where $R_t = 1$ can be sustained with a level of social distancing that is not too costly, optimal policy stabilizes the infection rate at a low level. The initial wave of infections shifts optimal costs away from reduced activity and towards health costs.

We now discuss each of the modifications in turn, along with its impact on the dynamics of the pandemic.

Alternative Utility Function In Figure 14, we modify the utility function to $u(a) = -\frac{1}{2}(1-a)^2$. This leaves $u(1) = u'(1) = 0$ and also leaves $u''(1)$ unchanged. The latter assumption ensures the value of a statistical life is unchanged. However, it implies less curvature in the utility function and in particular that $u'(0)$ is finite. This modification reduces the marginal value of social activity, and so both equilibrium and optimal social activity fall with this calibration. Still, all of our takeaway messages hold with this calibration. Optimal policy has an immediate and sustained reduction in social activity, although the extent of it is limited and so the effective reproduction number remains close to 1.

Cost of Disease Here we show the results for $\kappa = 98.5$, that is we cut our baseline parameter value of the expected cost of infection in half. This can be viewed as capturing a lower infection fatality rate or a lower VSL. We show the resulting dynamics for optimum and laissez-faire in Figure 15.

Cutting the cost of infection increases the peak equilibrium infection rate. The peak optimal infection rate increases by a much larger amount, from a very low level of 0.07 percent to a peak close to equilibrium. The delay induced by the optimal policy is also decreased considerably, and the peak of the infection rate under optimal policy is less than 100 days after the equilibrium peak. With a lower VSL, the cost of persistent social distancing exceeds its health care returns.[21]

Higher Duration of Infectivity and Higher R_0 Some authors use a considerably longer duration of infectivity $\frac{1}{\gamma}$. For instance, Hall, Jones and Klenow (2020) set $\gamma = \frac{1}{18}$. We follow them here but maintain the target of a 30 percent daily growth rate in a world without social distancing. We therefore adjust $\beta = 0.3 + \frac{1}{18}$. This gives a substantially higher basic reproduction number of $R_0 = 6.4$.

[21] In this case, as in several of the following, it happens that at times N_i under the optimum exceeds that of laissez-faire. This does not necessarily imply that there is excessive social distancing under laissez-faire. It might instead reflect the state variables having evolved differently up to such a point, with many more susceptibles left under the optimum. See the case with a lower cure probability below, however, for a case with excessive individual shielding.

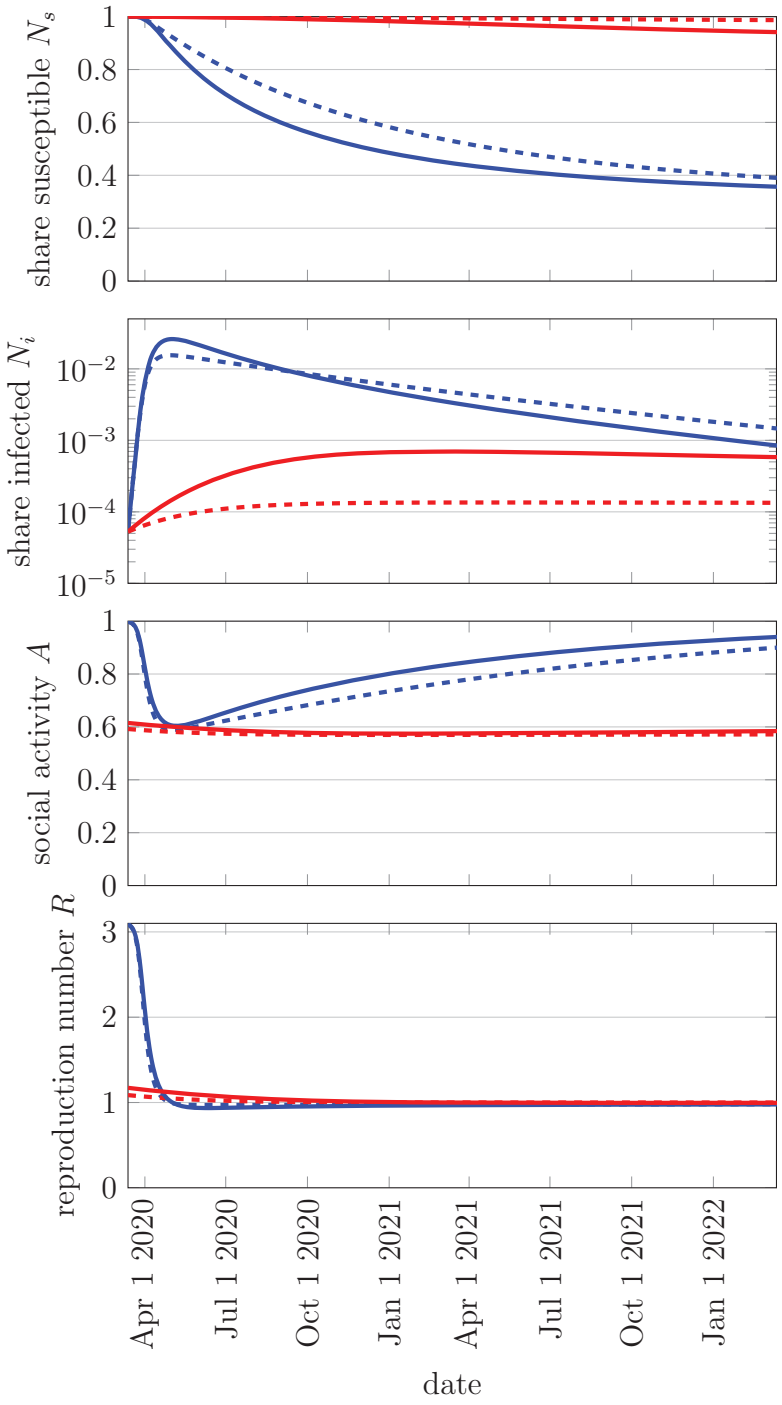

Notes: See Table 1 for calibration. Only change: We assume the utility from social activity is $u(a) = -\frac{1}{2}(1-a)^2$. Solid lines show the baseline calibration and dashed lines show the robustness check. The second plot is drawn on a log scale.

Figure 14: Optimal Policy vs Laissez-Faire with quadratic utility.

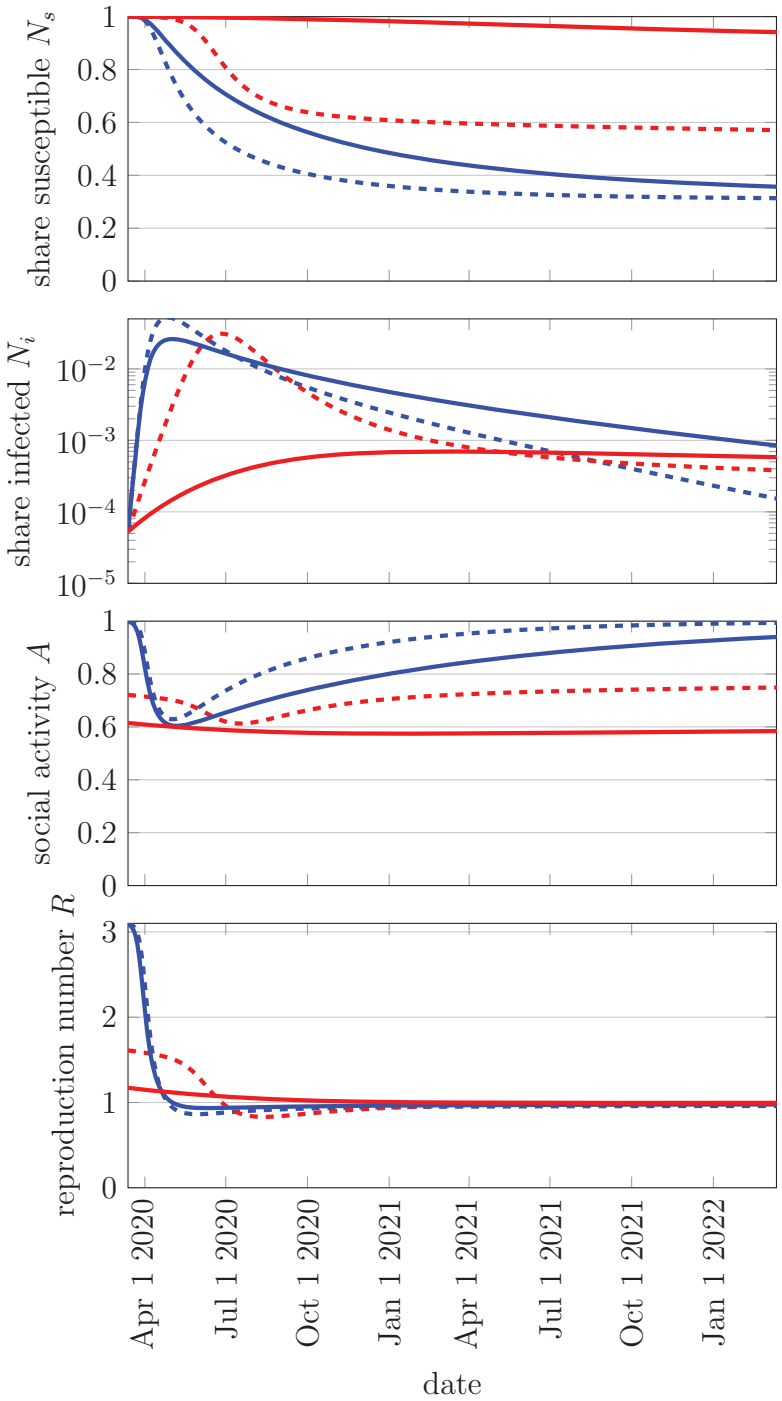

Notes: See Table 1 for calibration. Only change: We set $\kappa = 98.5$ instead of $\kappa = 197$. Solid lines show the baseline calibration and dashed lines show the robustness check. The second plot is drawn on a log scale.

Figure 15: Optimal Policy vs Laissez-Faire with low cost of infection.

We report the corresponding results in Figure 16. This has qualitatively little impact on the results, but there are significant quantitative differences. Most noticeably, with a much higher basic reproduction number, social distancing is less effective at reducing the infection rate. The peak infection rate in equilibrium is substantially elevated. Even more noticeably, optimal policy now allows for a substantial wave of infections, since the cost of suppressing it is prohibitive. Conversely, both equilibrium and optimal policy see an even larger contraction of social activity. In either case, optimal policy still keeps $R(t)$ marginally below 1 after peak infections.

Lower Cure Probability We have so far assumed that the expected time until a cure is 1.5 years. Figure 17 shows what happens if we double this to 3 years. The laissez-faire equilibrium dynamics are effectively the same, reflecting the fact that individuals are insensitive to the discount rate, and difficulties in finding a cure are equivalent to a reduction in discounting. The dynamics of the disease, however, differ sharply under the optimal policy. In particular, the planner allows a substantial wave of infections to occur, so the expected number of sick (and hence fatalities) rises much more quickly. This reflects a reduction in the benefits of delay.

Still, the path of optimal policy does not change qualitatively. Immediate and long-lasting social distancing is optimal but the optimal effective reproduction number stays close to 1 after peak infections.

Finally, if $\delta \to 0$ and there is no hope for a cure, the externalities might actually reverse. Since there is no hope for a cure, the planner lets the population rapidly reach herd immunity, where the pandemic necessarily ends. In laissez-faire, however, a "rat race to shield" (Garibaldi, Moen and Pissarides, 2020) occurs. Individuals engage in excessive social distancing in the hope of being one of the remaining susceptibles once herd immunity is reached.

Stock of Initially Infected We have experimented with the stock of the initially infected for several reasons. First, one might think that as the fraction of initially infected individuals becomes exceedingly small one of our key policy lessons—that the optimal policy immediately curtails social activity to buy time—no longer holds. This is indeed true in the limit: for $N_i(0)$ small enough, the expected uncurtailed outbreak date is so far in the future that the (social) gains from social distancing must vanish. However, suppose we start with $N_i(0) = 1/7 \cdot 10^9$, i.e. patient zero, a natural lower bound on the initial seed. With $\beta - \gamma = 0.3$, in just 30 days $N_i(t)$ exceeds 10^{-6} if there is no social distancing. The delay motive we have appealed to above therefore remains quantitatively powerful.

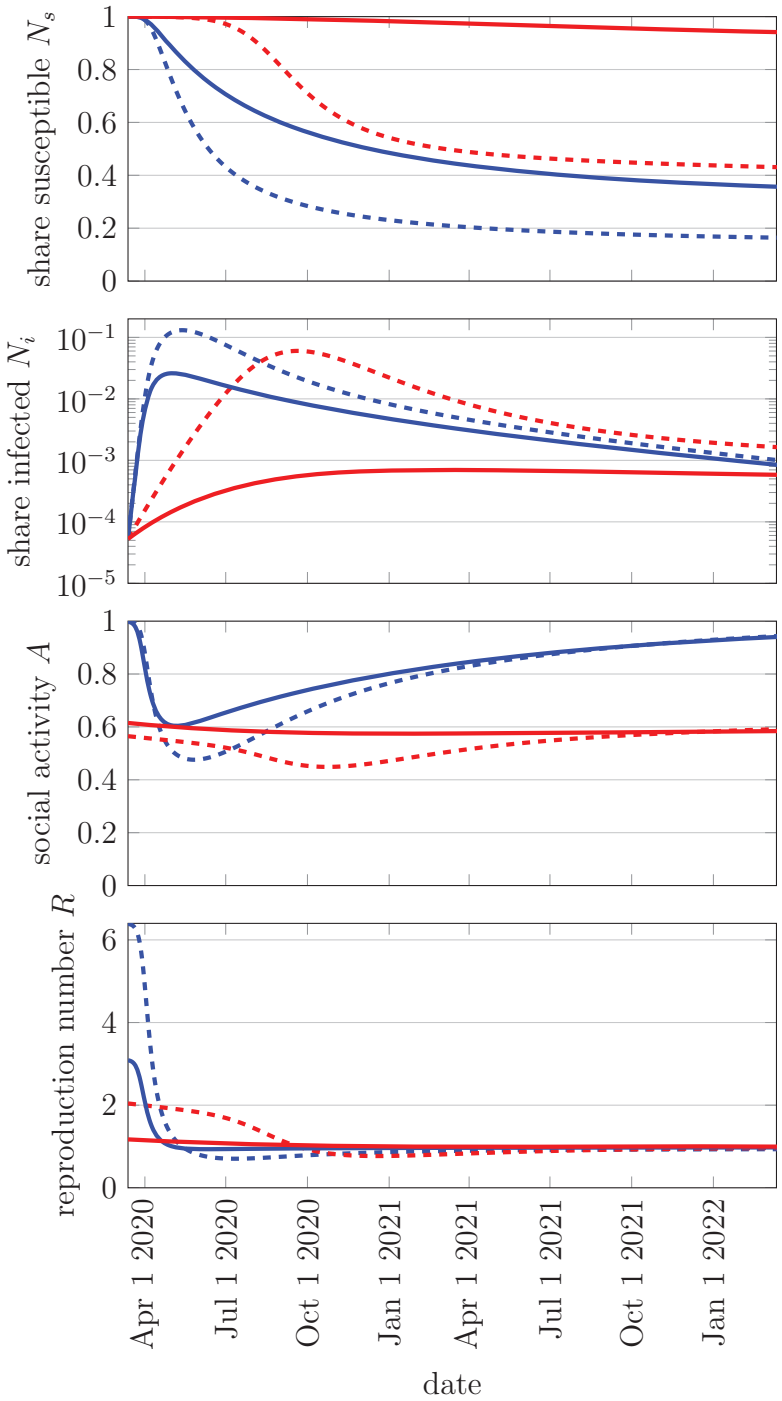

Notes: See Table 1 for calibration. Only change: We set $\gamma = 0.056$ (instead of $\gamma = 0.143$) and $\beta = 0.356$ such that $R_0 = 6.4$ (instead of 3.1). Solid lines show the baseline calibration and dashed lines show the robustness check. The second plot is drawn on a log scale.

Figure 16: Optimal Policy vs Laissez-Faire with long duration of infectivity.

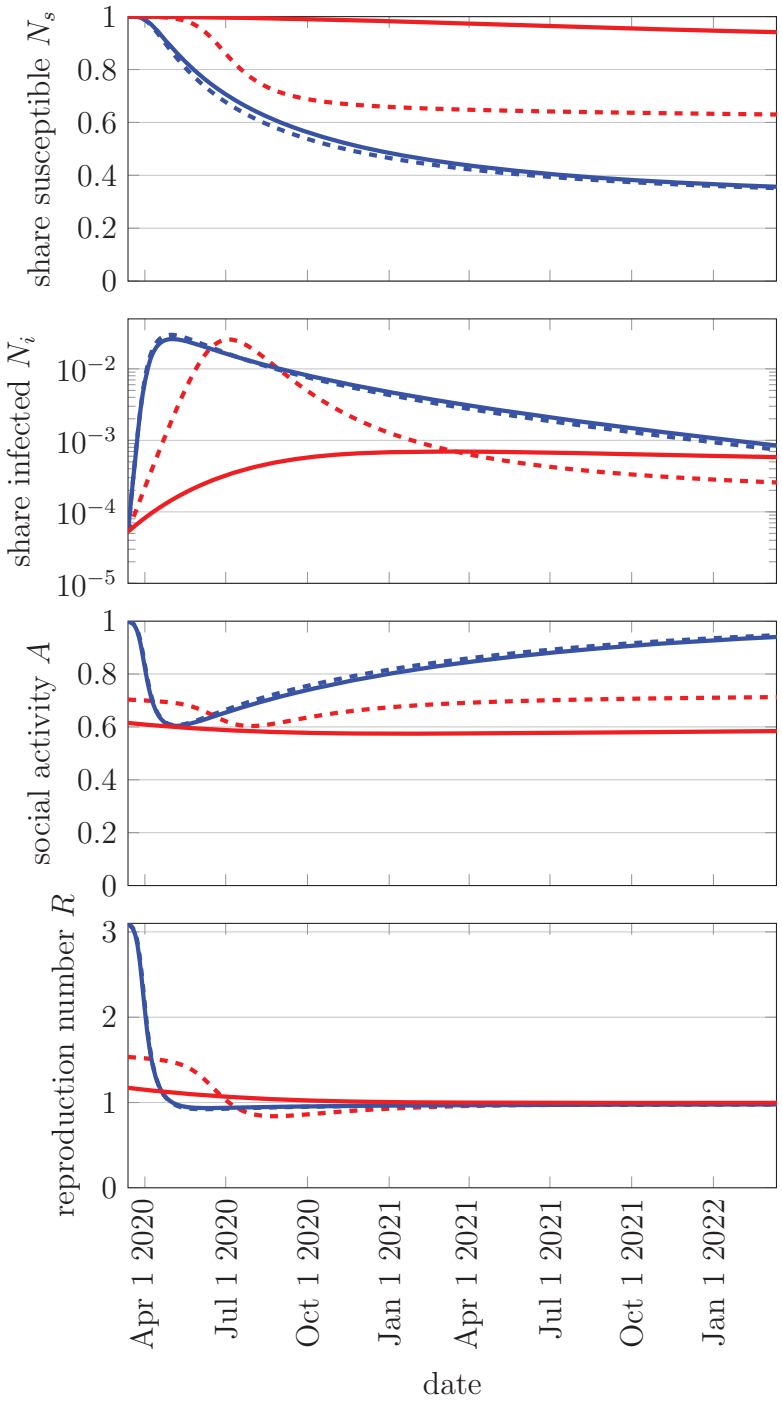

Notes: See Table 1 for calibration. The only change is that we set $\delta = \frac{0.33}{365}$ (instead of $\frac{0.67}{365}$). Solid lines show the baseline calibration and dashed lines show the robustness check. The second plot is drawn on a log scale.

Figure 17: Optimal Policy vs Laissez-Faire with low probability of cure.

Second, we have also substantially increased $N_i(0)$ up to 1 percent. This could for instance capture the situation in places where COVID-19 appeared first, or it could capture the situation in places where the initial policy response was botched or individuals did not respond because of, say, false information. We plot the corresponding time paths for equilibrium and optimum in Figure 18.

The qualitative patterns are largely unchanged but the optimal policy acts more aggressively. An important observation, shown in the bottom panel of the figure, is that in this case optimal policy suppresses social activity immediately to such an extent that $N_i(t)$ falls from the outset. As a consequence of the high initial stock of infections, the planner has less room to delay the wave of infections and so drives down the stock of infections from the outset. Nonetheless, optimal policy monotonically relaxes social distancing, ultimately relying on a reduction in the share of susceptible individuals for the continued decline in infections. The equilibrium time path, in turn, remains largely unchanged. Starting with more infections just shifts it ahead in time.

C.2 Imperfect Information about Recovery

Throughout the paper, we have assumed that people know when they have recovered from the disease and that recovery confers lifelong immunity. This implies that the recovered's choice of social activity is unaffected by the pandemic, $a_r(t) = A_r(t) = a^* = 1$. Here we relax part of that assumption. We still assume that recovery confers lifelong immunity, but we assume that some infected people never learn that they are infected.

More precisely, we allow for three states following an infection. First, with probability $\zeta \in [0,1]$, the person recovers without realizing he was sick, entering a new state z. Second, with probability $(1-\zeta)\pi \in [0,1]$, the individual dies and pays a cost v. Third, with probability $(1-\zeta)(1-\pi) \in [0,1]$, the person recovers and knows he has lifetime immunity, moving to state r. Susceptible, infected, and recovered individuals who do not know they were sick all have the same information and so must choose the same level of social activity $a(t)$. Similarly, the social planner applies any social distancing requirements to all these individuals. In contrast, recovered individuals who know they were sick can choose a different level of activity $a_r(t)$. The baseline model is a special case with $\zeta = 0$.

The expected mortality cost of the disease is now $\kappa = (1-\zeta)\pi v$. In a laissez-faire equilibrium, individuals maximize

$$\max_{\{a(t),a_r(t)\}} \int_0^\infty e^{-(\rho+\delta)t}\big((n_s(t)+n_i(t)+n_z(t))u(a(t)) + n_r(t)u(a_r(t)) - \gamma n_i(t)\kappa\big)dt$$

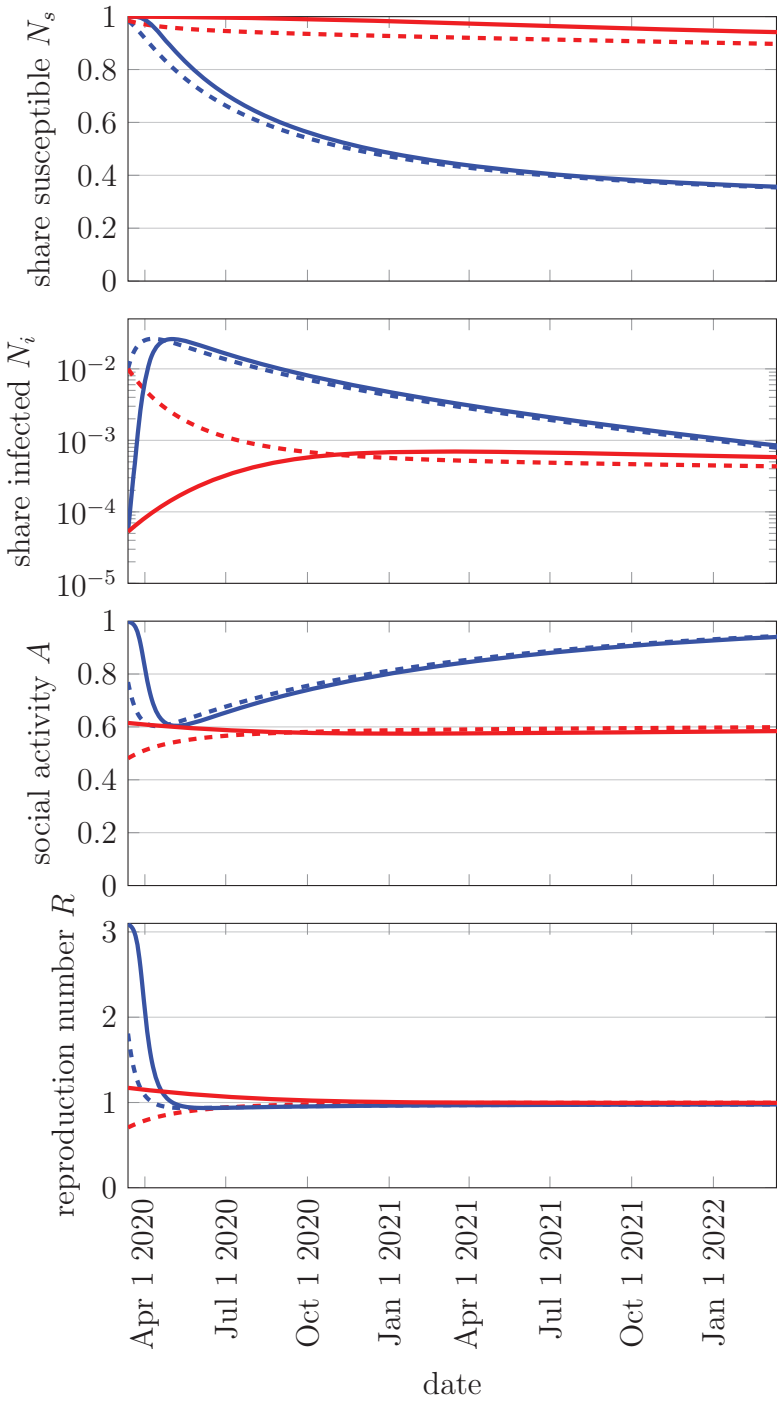

Notes: See Table 1 for calibration. Only change: We set $N_i(0) = 10^{-2}$ instead of $N_i(0) = 0.0000527$. This also reduces the initial value of $N_s(0)$ to 0.985 instead of 0.9999223. Solid lines show the baseline calibration and dashed lines show the robustness check. The second plot is drawn on a log scale.

Figure 18: Optimal Policy vs Laissez-Faire with higher stock of initially infected.

subject to unchanged law of motions for n_s and n_i, equations (7) and (8). As before, it is optimal to set $a_r(t) = 1$ so $u(a_r(t)) = 0$. We thus drop this control variable.

While in principle we could introduce another law of motion for n_z, the following observation avoids the need to do that: at any point in time, a constant fraction ζ of the individuals who are neither susceptible nor infected are in state z, recovered without realizing they were sick. This implies that $n_z(t) = \zeta(1 - n_s(t) - n_i(t))$ and hence $n_s(t) + n_i(t) + n_z(t) = \zeta + (1-\zeta)(n_s(t) + n_i(t))$ for all t.[22]

Putting this together, the Hamiltonian can then be written as

$$\begin{aligned} H(n_s(t), n_i(t), a(t), \lambda_s(t), \lambda_i(t)) = \big(\zeta + (1-\zeta)(n_s(t) + n_i(t))\big)u(a(t)) - \gamma n_i(t)\kappa \\ - \lambda_s(t)\beta a(t) n_s(t) A(t) N_i(t) + \lambda_i(t)\big(\beta a(t) n_s(t) A(t) N_i(t) - \gamma n_i(t)\big). \end{aligned}$$

The static first order condition is

$$\big(\zeta + (1-\zeta)(n_s(t) + n_i(t))\big)u'(a(t)) = (\lambda_s(t) - \lambda_i(t))\beta n_s(t) A(t) N_i(t). \tag{23}$$

The derivatives with respect to the state variables $n_s(t)$ and $n_i(t)$ are

$$(\rho + \delta)\lambda_s(t) - \lambda_s'(t) = (1-\zeta)u(a(t)) + (\lambda_i(t) - \lambda_s(t))\beta a(t) A(t) N_i(t), \tag{24}$$

$$(\rho + \delta)\lambda_i(t) - \lambda_i'(t) = (1-\zeta)u(a(t)) - \gamma\big(\kappa + \lambda_i(t)\big). \tag{25}$$

The transversality conditions are unchanged

$$\lim_{t\to\infty} e^{-(\rho+\delta)t}\lambda_s(t) n_s(t) = \lim_{t\to\infty} e^{-(\rho+\delta)t}\lambda_i(t) n_i(t) = 0. \tag{26}$$

As usual, we impose the equilibrium restrictions $a(t) = A(t)$, $n_s(t) = N_s(t)$, and $n_i(t) = N_i(t)$ to get a set of differential equations that can be solved with the state equations (7) and (8).

The Hamiltonian for the planner is

$$\begin{aligned} H(N_s(t), N_i(t), A(t), \mu_s(t), \mu_i(t)) = \big(\zeta + (1-\zeta)(N_s(t) + N_i(t))\big)u(A(t)) \\ - \gamma N_i(t)\kappa - \mu_s(t)\beta A(t)^2 N_s(t) N_i(t) + \mu_i(t)\big(\beta A(t)^2 N_s(t) N_i(t) - \gamma N_i(t)\big). \end{aligned}$$

The necessary first order condition with respect to the control A is

$$\big(\zeta + (1-\zeta)(N_s(t) + N_i(t))\big)u'(A(t)) = 2(\mu_s(t) - \mu_i(t))\beta A(t) N_i(t) N_s(t), \tag{27}$$

[22] This result assumes that $n_z(0) = \zeta(1 - n_s(0) - n_i(0))$, so the relationship holds at the initial value of the state variables. Given the model structure, this restriction seems innocuous.

while the necessary costate equations are

$$(\rho+\delta)\mu_s(t) - \mu_s'(t) = (1-\zeta)u(A(t)) + (\mu_i(t)-\mu_s(t))\beta A(t)^2 N_i(t), \tag{28}$$

$$(\rho+\delta)\mu_i(t) - \mu_i'(t) = (1-\zeta)u(A(t)) + (\mu_i(t)-\mu_s(t))\beta A(t)^2 N_s(t) - \gamma\big(\kappa+\mu_i(t)\big). \tag{29}$$

Finally, the planner also has unchanged necessary tranversality conditions

$$\lim_{t\to\infty} e^{-(\rho+\delta)t}\mu_s(t)N_s(t) = \lim_{t\to\infty} e^{-(\rho+\delta)t}\mu_i(t)N_i(t) = 0. \tag{30}$$

Again, we solve these differential equations with the state equations (7) and (8).

Figure 19 shows the results in the extreme case where $\zeta = 1-\pi$, so individuals who survive the disease are never aware that they were even sick. Compared to the benchmark model, people increase their social activity under laissez-faire when susceptible or infected. This reflects the fact that as the disease progresses, they are increasingly likely to have acquired immunity. In contrast, the optimal policy suppresses activity when the planner is unaware of recovery status. This reflects the opposing force, that acquiring immunity is less valuable when people who are immune must also be subject to social distancing requirements.

C.3 Hospitalization

It is straightforward to extend the model in Appendix C.2 to allow for hospitalization. When the infectious period ends, at rate γ, two events can happen. First, with probability ζ, the individual never learns that he was sick, and so enters state z. With complementary probability he enters the hospital. The disease then resolves itself in the hospital at rate ξ, ending either with death with probability π and recovery with probability. Thus the ex ante death probability is still $(1-\zeta)\pi$.

As stated, there are only two relevant changes introduced by hospitalization. First, at the time the infectious period ends, the expected cost of the disease is $\kappa = (1-\zeta)\pi\xi v/(\rho+\xi)$, slightly less than $(1-\zeta)\pi v$ which reflects the fact that the disease resolves itself at rate ξ once in the hospital. In practice, this change is unlikely to be quantitatively relevant. Second, in the baseline model, the death rate always moves proportionately with the number of infectious people. The hospitalization period introduces an empirically relevant lag between the peak of infections and the peak of mortality, with the share of hospitalized people evolving as $n_h'(t) = \gamma n_i(t) - \xi n_h(t)$ and the cumulative number of deceased people satisfying $n_d'(t) = \pi\xi n_h(t)$. This is only relevant for the exact timing of deaths, not for either the equilibrium or optimal policy given a value of κ.

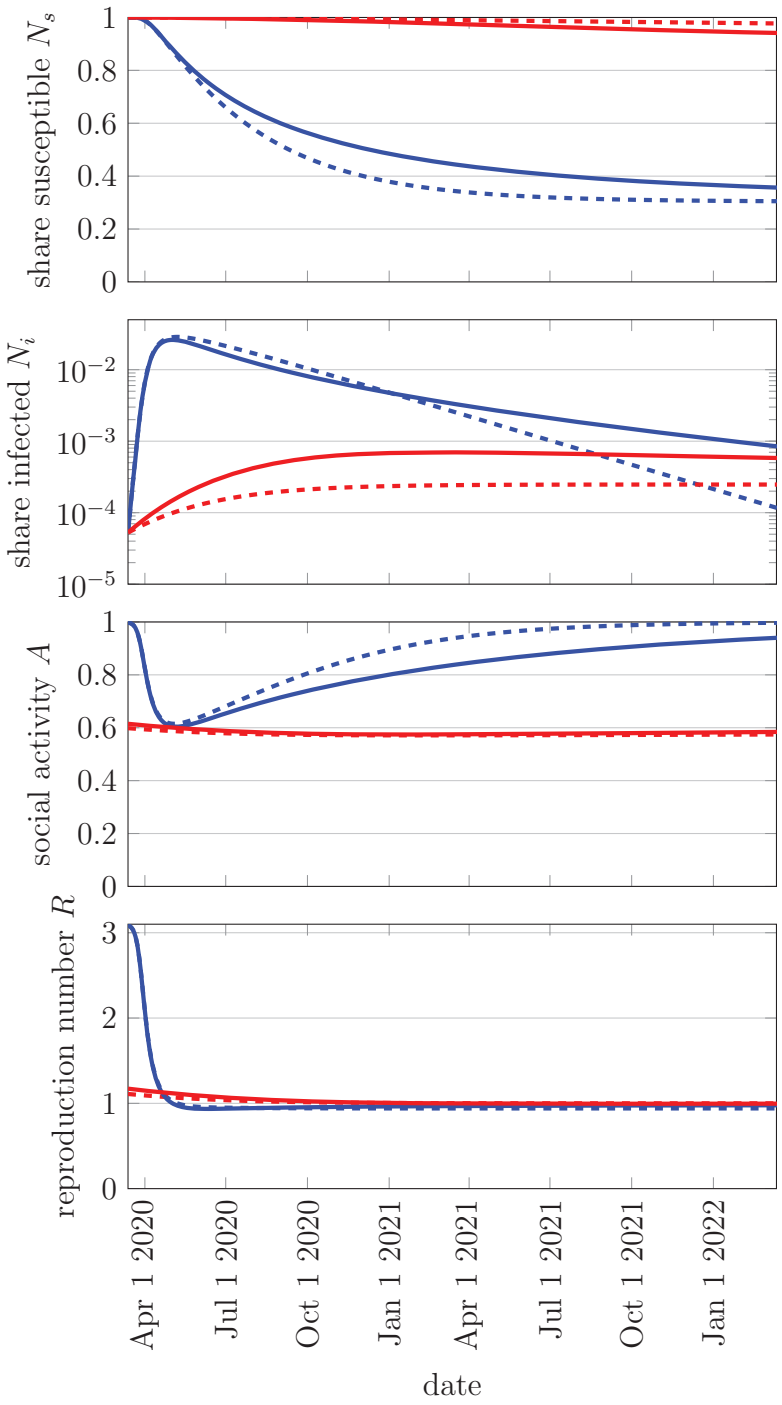

Notes: See Table 1 for calibration. Only change: We set $\zeta = 1 - \pi$, so individuals do not know their recovery status. Solid lines show the baseline assumption ($\zeta = 0$) and dashed lines show the robustness check. The second plot is drawn on a log scale.

Figure 19: Optimal Policy vs Laissez-Faire when individuals do not know whether they have recovered.

D Second Wave(s)

The US and most other countries on the Northern hemisphere witnessed a large rise in cases in the winter of 2020–21. Our model, however, predicts that, following the initial peak of infections, infections will slowly roll over under both optimum and equilibrium. We believe the discrepancy has much to do with time-varying parameters that reflect both seasonality and the arrival of new mutants and will next provide and extension of the model to capture these. However, a similar discrepancy already shows in the early summer 2020 when the US, like many other countries, experienced a second wave of infections. We believe that is primarily a consequence of time-varying and sub-optimal policies, reflecting that the US largely abolished mandatory restrictions on mobility in the late spring of 2020, and note that, in principle, the baseline model can already account for a second wave by incorporating sub-optimal policies. Here, however, we focus on seasonality and mutants as the main culprits.

The following simple model extension can accommodate an additional wave of infections and reductions in activity. In particular, we depict the evolution of the pandemic in the model under the following circumstances. For 210 days after its onset on March 13th, the pandemic evolves according to the model as described previously. Then on October 9th, a shock to the transmission rate β occurs, with β permanently rising by fifty percent. We think of this shock as capturing the arrival of new mutants and seasonality. Importantly, we assume that this shock remained unobserved for three weeks. Because of that, social activity during those three weeks evolved as if the pandemic had continued under the old parameters, both in the equilibrium and in the optimum. We then assume that individuals became aware of the new parameters three weeks later, on Oct 30th. From then on, individuals and policy makers behaved as previously described, but with new parameter values.

We think of this as a natural way of picking up the notion that most observers seem not to have forecast the jump in cases in the US and in Europe that occurred in the fall. In particular, while certainly many had voiced concern over seasonality, the strength of the second wave of infections surprised most. Consistently, there is now agreement that policy acted "too late" in the fall of 2020.

We plot the evolution of the pandemic under this scenario in Figure 20. Under both equilibrium and optimum, the stock of infections starts rising rapidly as soon as the shock occurs, albeit off a much lower level under the formerly optimal policy. Once aware of the shock, social activity falls in both equilibrium and optimum.

The optimal policy then admits a sharp rise in infections that levels off in mid January and from there on, like before, keeps rolling over the stock of infections. The fourth panel of Figure 20 illustrates the evolution of the effective reproduction number during the second

wave: $R(t)$ first exceeds 1 and then falls slightly below, before converging back to 1. This is similar to the deviation of $R(t)$ from 1 observed during the large wave of infections in the fall and winter of 2020–21, depicted in Figure 5.

This exercise has many degrees of freedom, and so we view it largely as a proof of concept, not a definitive quantitative description of the second wave of the pandemic. Nonetheless, it shows that the model can readily admit extensions that are both realistic and capable of quantitatively picking up some of the swings the pandemic has thus far displayed.

References

Goolsbee, Austan and Chad Syverson, "Fear, Lockdown, and Diversion: Comparing Drivers of Pandemic Economic Decline 2020," 2020.

Hall, Robert E., Charles I. Jones, and Peter J. Klenow, "Trading off Consumption and COVID-19 Deaths," 2020.

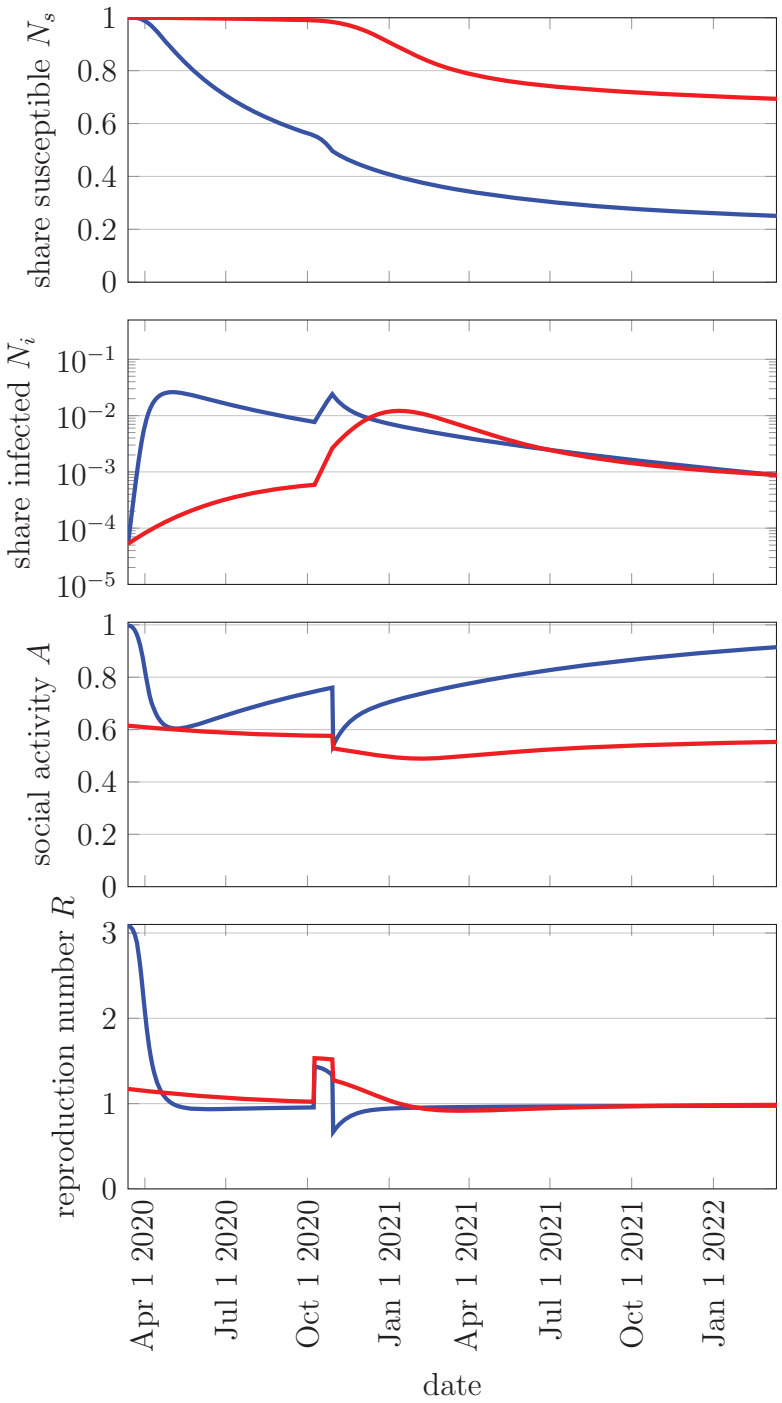

Notes: Baseline calibration up until Oct 9th. Then β increases by 50%. Both optimum and equilibrium activity continues for 20 days under the previously optimal plan. It then optimally adjusts to the new parameters and state variables.

Figure 20: Laissez-Faire and Optimal Policy with seasonality and/or mutants.